



UNIVERSITY OF LEEDS

This is a repository copy of *Elastoplastic solution for cylindrical cavity contraction in unsaturated soils*.

White Rose Research Online URL for this paper:

<https://eprints.whiterose.ac.uk/208401/>

Version: Accepted Version

Article:

Zhang, J.-L., Sun, E.-C., Zhuang, P.-Z. et al. (2 more authors) (2024) Elastoplastic solution for cylindrical cavity contraction in unsaturated soils. *Géotechnique Letters*, 14 (1). pp. 1-7. ISSN 2045-2543

<https://doi.org/10.1680/jgele.23.00080>

Reuse

Items deposited in White Rose Research Online are protected by copyright, with all rights reserved unless indicated otherwise. They may be downloaded and/or printed for private study, or other acts as permitted by national copyright laws. The publisher or other rights holders may allow further reproduction and re-use of the full text version. This is indicated by the licence information on the White Rose Research Online record for the item.

Takedown

If you consider content in White Rose Research Online to be in breach of UK law, please notify us by emailing eprints@whiterose.ac.uk including the URL of the record and the reason for the withdrawal request.



eprints@whiterose.ac.uk
<https://eprints.whiterose.ac.uk/>

Elastoplastic solution for cylindrical cavity contraction in unsaturated soils under constant suction conditions

Mr Jia-Liang **Zhang**¹, Postgraduate Student Email: zhangjialiang@mail.sdu.edu.cn;

Mr En-Ci **Sun**¹, Postgraduate Student Email: sunenci@mail.sdu.edu.cn;

Prof Pei-Zhi **Zhuang**¹ Email: zhuangpeizhi@sdu.edu.cn;

Prof Hai-Sui **Yu**², FEng E-mail: H.Yu@leeds.ac.uk;

Mr He **Yang**², PhD Candidate E-mail: yanghesdu@mail.sdu.edu.cn;

¹School of Qilu Transportation, Shandong University, Jinan, 250002, China

²School of Civil Engineering, University of Leeds, Leeds, LS2 9JT, UK

Abstract: This letter develops an elastoplastic solution for cylindrical cavity contraction in unsaturated soils under constant suction conditions. The elastoplastic cavity contraction problem is formulated into a set of first-order ordinary differential equations (ODEs) by introducing a new auxiliary variable, which is solved as an initial value problem. The new solution is validated by comparison with numerical simulation results. Finally, parametric studies show that, as soil suction increases, the internal support pressure decreases faster with cavity contraction, the unloading-induced plastic zone becomes narrower, and **the changes in effective stresses are smaller for a given tunnel convergence.**

Keywords: Ground response curve; unsaturated soil; cavity contraction; **tunnels & tunnelling; plasticity; stress analysis**

23 Introduction

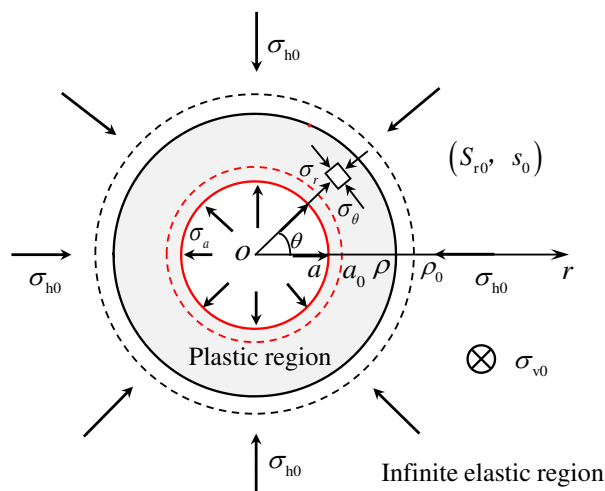
24 The relationship between support pressure and tunnel convergence (i.e. ground response curve, GRC) is vital
25 for tunnel design with the convergence-confinement method (Brown et al. 1983; Park et al. 2008). Very often
26 GRC is predicted by the elastoplastic cavity contraction theory that studies the development of stresses and
27 displacement around a contracting cylindrical cavity (Yu 2000). For example, a number of cavity contraction
28 solutions were available for soils and rocks with various constitutive models, such as the Mohr-Coulomb
29 model (Yu and Rowe 1999; Carranza-Torres 2003; Vrakas and Anagnostou 2014), Hoek-Brown failure criteria
30 (Brown et al. 1983; Zareifard 2020; Guan et al. 2022; Cai et al. 2023), strain hardening/softening Drucker-
31 Prager model (Chen et al. 2012; Chen and Abousleiman 2017), and critical state (Cam Clay) models (Yu and
32 Rowe 1999; Chen and Abousleiman 2016; Mo and Yu 2017; Zhuang et al. 2020). Also, some cavity contraction
33 solutions were developed to investigate the influence of soil anisotropy (Chen H et al. 2022), ground surface
34 (Zhuang et al. 2022), non-hydrostatic in-situ stress field (Ma et al. 2023), seepage pressure (Sun et al. 2023;
35 Zhao et al. 2023), and plane stress conditions (Yang et al. 2022) on the characteristics of GRCs.

36 Soils in the region affected by groundwater and rainfall are normally in an unsaturated state. GRC for
37 tunnelling in unsaturated soils ought to be affected by suction and degree of saturation. However, to the best
38 knowledge of the authors, cavity contraction solutions for unsaturated soils have not been reported yet. To fill
39 the gap, this letter provides an elastoplastic solution for cavity contraction in unsaturated soils under constant
40 suction conditions. The work is an extension of Chen H et al. (2020) to the cavity contraction scenario, and a
41 modified auxiliary variable is introduced to transform the governing equations into a set of first-order ordinary
42 differential equations (ODEs). Finally, a parametric study is conducted to highlight the influence of suction
43 on GRC, stress paths, and stress distributions.

44 Problem Definition and Assumptions

45 This letter considers the contraction of a cylindrical cavity with an initial radius a_0 and infinite length in the
46 axial direction, as shown in Figure 1. The soil around the cavity is of infinite radial extent and is modelled by
47 an elastoplastic unsaturated model. Prior to unloading (i.e. initial state), total horizontal and vertical stresses
48 (σ_{h0} , σ_{v0}) act throughout the soil, and the initial suction and degree of saturation are s_0 and S_{r0} ,
49 respectively. Note that the initial stress state is shown in a general form in order to extend the potential
50 applications of the solution, and it can be assumed that $\sigma_{h0} = \sigma_{v0}$ for tunnelling and $\sigma_{h0} \neq \sigma_{v0}$ for other

51 excavation problems such as wellbore drilling (Chen and Abousleiman 2016; Chen and Abousleiman 2017;
 52 Chen S et al. 2022). Then the internal support pressure gradually reduces from σ_{h0} to σ_a , while the radius
 53 of the inner cavity reduces from a_0 to the current radius a . In the contraction process, an unloading-induced
 54 plastic zone forms in the region of $a \leq r \leq \rho$, where ρ is the current radius of the elastoplastic boundary.
 55 For convenience the present cavity contraction problem is accounted for by the cylindrical polar coordinates
 56 (r, θ, z) with the origin at the cavity centre.



57
 58 **Figure 1 Schematic of the cylindrical cavity contraction problem**

59 The following commonly used assumptions are adopted for the theoretical analysis of cavity contraction in
 60 homogenous and isotropic soils, including (Brown et al. 1983; Yu 2000; Xu and Xia 2021):

- 61 (a) The plane strain assumption is satisfied for a long tunnel.
- 62 (b) The stresses and geometry boundary conditions are axisymmetric.
- 63 (c) The unloading process is sufficiently slow so that the dynamic effect can be neglected.

64
 65 Taking compressive stresses/strains as positive, the equilibrium equation and boundary conditions for the
 66 axisymmetric problem can be expressed as

67
$$\frac{d\sigma_r}{dr} + \frac{\sigma_r - \sigma_\theta}{r} = 0 \quad (1)$$

68
$$\sigma_r|_{r=a} = \sigma_a \quad (2)$$

69
$$\sigma_r|_{r=\infty} = \sigma_{h0} \quad (3)$$

70 where σ_r and σ_θ denote the total radial and circumferential stresses, respectively; $d(\bullet)$ denotes the

spatial differential of (\bullet) for a given time (i.e. Eulerian description); r denotes the current radial position of a soil particle (i.e. material point).

Constitutive modelling of unsaturated soils

The unsaturated critical state model (UCSM) of Sun et al. (2007) is adopted for constitutive modelling of unsaturated soils, which is briefly introduced as follows. In UCSM the effective stress (i.e. average soil skeleton stress) and suction are selected as two stress state variables, defined as

$$\sigma'_{ij} = \sigma_{ij} - u_a \delta_{ij} + S_r s \delta_{ij} \quad (4)$$

$$s = u_a - u_w \quad (5)$$

where σ'_{ij} =effective stress tensor; σ_{ij} =total stress tensor; δ_{ij} =Kronecker's delta; S_r =degree of saturation; s =suction; u_a =pore air pressure (is assumed to equal the atmospheric pressure); u_w =pore water pressure.

In the $p'-q$ plane UCSM shares the same yield surface shape with the modified Cam Clay model (MCC) as shown in Eq. (6) and Figure 2:

$$f = (\eta/M)^2 - [p'_y(s)/p' - 1] = 0 \quad (6)$$

$$p'_y(s) = p'_n \left(\frac{p'_y(0)}{p'_n} \right)^{\frac{\lambda(0)-\kappa}{\lambda(s)-\kappa}} \quad (7)$$

$$\lambda(s) = \lambda(0) [(1-b)e^{-cs} + b] \quad (8)$$

where f denotes the yield function; $\eta = q/p'$ is the stress ratio; $p' = \sigma'_{ii}/3$ denotes the mean effective stress; $q = \sqrt{3(\sigma'_{ij} - p'\delta_{ij})(\sigma'_{ij} - p'\delta_{ij})}/2$ is the deviatoric stress; M denotes the slope of the critical state line (CSL) in the $p'-q$ plane; $p'_y(s)$ is the isotropic yield stress at a suction of s ; p'_n is a reference stress; $\lambda(s)$ and $\lambda(0)$ are the slopes of the normal compression line in the $v - \ln p'$ plane at suctions of s and 0, respectively; κ is the slope of the swelling line in the $v - \ln p'$ plane (independent on suction); $p'_y(0)$ is the isotropic consolidation pressure at a suction of 0 (i.e. saturated soils); b and c are two material parameters for unsaturated soils (Alonso et al. 1990).

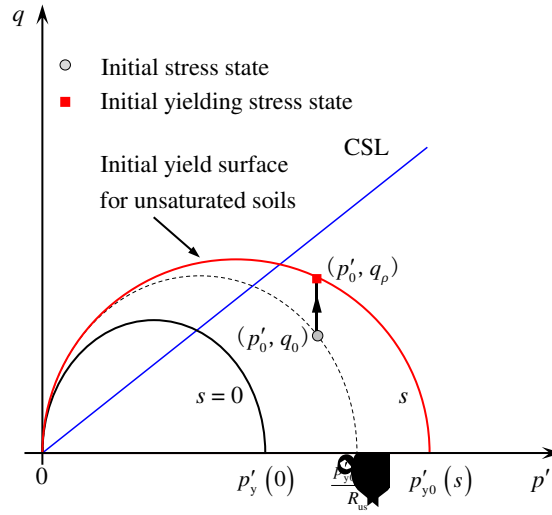


Figure 2 Yield surface in the $p'-q$ plane.

An associate flow rule and the volumetric hardening law are used in USCM, and the plastic volumetric strain ε_v^p satisfies:

$$D\varepsilon_v^p = \frac{\lambda(0) - \kappa}{v} \frac{Dp'_y(0)}{p'_y(0)} \quad (9)$$

where $D(\bullet)$ denotes the material time differential of (\bullet) for a given soil particle (i.e. Lagrangian description).

Under constant suction conditions, the soil water retention curve in Sun et al. (2007) can be simplified as

$$DS_r = -\lambda_{sc} Dv \quad (10)$$

where v = specific volume of unsaturated soils; λ_{sc} = slope of the $S_r - v$ curve at a constant suction.

Elastoplastic Solution

Solution in the elastic region

In the elastic region ($r > \rho$) the stress-strain relationship is assumed to obey Hooke's law and small strain definitions (Yu 2000; Chen H et al. 2020):

$$\begin{bmatrix} D\varepsilon_r^e \\ D\varepsilon_\theta^e \\ D\varepsilon_z^e \end{bmatrix} = - \begin{bmatrix} d(Du)/dr \\ Du/r \\ 0 \end{bmatrix} = \frac{1}{E} \begin{bmatrix} 1 & -\mu & -\mu \\ -\mu & 1 & -\mu \\ -\mu & -\mu & 1 \end{bmatrix} \begin{bmatrix} D\sigma_r' \\ D\sigma_\theta' \\ D\sigma_z' \end{bmatrix} \quad (11)$$

where ε_r^e , ε_θ^e and ε_z^e denote the elastic radial, circumferential, and vertical strains, respectively; σ_r' , σ_θ' ,

109 and σ'_z denote the radial, circumferential, and vertical effective stresses, respectively; $u = r - r_0$ represents
 110 the radial displacement of a soil particle whose initial radial position is r_0 ; E and μ are the elastic
 111 modulus and Poisson's ratio of soils, and E is expressed as

$$112 \quad E = \frac{3(1-2\mu)vp'}{\kappa} \quad (12)$$

113 Combining Eqs. (1), (3), (4) and (11), the solution for stresses, displacement, volume change, and
 114 saturation degree in the elastic zone can be obtained following Yu (2000) and Chen H et al. (2020):

$$115 \quad \sigma'_r = \sigma'_{h0} + (\sigma'_{r\rho} - \sigma'_{h0})(\rho/r)^2 \quad (13)$$

$$116 \quad \sigma'_\theta = \sigma'_{h0} - (\sigma'_{r\rho} - \sigma'_{h0})(\rho/r)^2 \quad (14)$$

$$117 \quad \sigma'_z = \sigma'_{v0} \quad (15)$$

$$118 \quad p' = p'_0 = \frac{\sigma'_{v0} + 2\sigma'_{h0}}{3} \quad (16)$$

$$119 \quad \frac{u}{r} = \frac{(1+\mu)}{E} (\sigma'_{r\rho} - \sigma'_{h0})(\rho/r)^2 \quad (17)$$

$$120 \quad v = v_0 \quad (18)$$

$$121 \quad S_r = S_{r0} \quad (19)$$

122 where σ'_{h0} and σ'_{v0} are the initial horizontal and vertical effective stress; p'_0 and v_0 are the initial mean
 123 effective stress and initial specific volume; $\sigma'_{r\rho}$ denotes the effective radial stress in the elastoplastic
 124 boundary and can be determined by substituting Eqs. (13)-(17) into the yield function (6) (Chen and
 125 Abousleiman 2013; Chen H et al. 2020), as

$$126 \quad \sigma'_{r\rho} = \sigma'_{h0} - \sqrt{[q_\rho^2 - (\sigma'_{h0} - \sigma'_{v0})^2]}/3 \quad (20)$$

$$127 \quad q_\rho = Mp'_0 \sqrt{p'_{y0}(s) - 1} \quad (21)$$

$$128 \quad p'_{y0}(s) = R_{us} p'_0 [1 + (q_0/Mp'_0)^2] \quad (22)$$

129 in which q_ρ denotes the deviatoric stress at $r = \rho$ and q_0 is the initial deviatoric stress; p'_{y0} is the initial
 130 isotropic pre-consolidation stress and R_{us} represents the initial overconsolidation ratio of unsaturated soils,

131 (see Fig. 2). Now the information at the elastoplastic boundary can be calculated by the elastic solution (Eqs.
 132 (13)-(22)), which provides initial values for solving the governing ODEs in the plastic region.

133 ***Solution in the plastic region***

134 Following Sun et al. (2007) and Chen H et al. (2020), the incremental stress-strain relationship for unsaturated
 135 elastoplastic soils can be expressed as

$$136 \begin{bmatrix} D\varepsilon_\theta \\ D\varepsilon_z \\ D\varepsilon_v \end{bmatrix} = \begin{bmatrix} B_{r\theta} & B_{\theta\theta} & B_{z\theta} \\ B_{rz} & B_{\theta z} & B_{zz} \\ B_{rp} & B_{\theta p} & B_{zp} \end{bmatrix} \begin{bmatrix} D\sigma'_r \\ D\sigma'_\theta \\ D\sigma'_z \end{bmatrix} \quad (23)$$

137 where

$$138 B_{r\theta} = -\frac{\mu}{E} + \frac{A_r A_\theta}{K_p} \quad (24)$$

$$139 B_{z\theta} = -\frac{\mu}{E} + \frac{A_z A_\theta}{K_p} \quad (25)$$

$$140 B_{rz} = -\frac{\mu}{E} + \frac{A_r A_z}{K_p} \quad (26)$$

$$141 B_{\theta z} = -\frac{\mu}{E} + \frac{A_\theta A_z}{K_p} \quad (27)$$

$$142 B_{\theta\theta} = \frac{1}{E} + \frac{A_\theta A_\theta}{K_p} \quad (28)$$

$$143 B_{zz} = \frac{1}{E} + \frac{A_z A_z}{K_p} \quad (29)$$

$$144 B_{kp} = \frac{\kappa}{3vp'} + \frac{A_k A_p}{K_p} \quad (k = r, \theta, z) \quad (30)$$

$$145 A_k = \frac{\partial f}{\partial \sigma'_k} = \frac{M^2 - \eta^2}{3M^2 p'} + \frac{3(\sigma'_k - p')}{M^2 p'^2} \quad (k = \theta, z) \quad (31)$$

$$146 A_p = \frac{\partial f}{\partial p'} = \frac{M^2 - \eta^2}{M^2 p'} \quad (32)$$

$$147 K_p = \frac{vp'_y(0)}{\lambda(s) - \kappa} \frac{M^2 - \eta^2}{M^2 p'^2} \left(\frac{p'_y(0)}{p'_n} \right)^{\frac{\lambda(0) - \lambda(s)}{\lambda(s) - \kappa}} \quad (33)$$

148 Note that the constitutive equation (23) is shown in the Lagrangian description while the equilibrium equation

149 (1) is in the Eulerian description. Following the pioneering work of Chen and Abousleiman (2013), Eq. (1)
 150 will be transformed into the expression of Lagrangian description by introducing a new auxiliary variable as
 151 follows.

152 The large deformation in the plastic region can be described by logarithmic strain definitions (Yu and
 153 Houlsby 1991; Yu 2000; Chen H et al. 2020), as

$$154 \quad \varepsilon_r = -\ln(dr/dr_0) \quad (34)$$

$$155 \quad \varepsilon_\theta = -\ln(r/r_0) \quad (35)$$

$$156 \quad \varepsilon_v = -\ln(v/v_0) = \varepsilon_r + \varepsilon_\theta \quad (36)$$

157 Combination of Eqs. (34)-(36) leads to the compatibility equation related to r and v :

$$158 \quad \frac{r_0 dr_0}{v_0} = \frac{r dr}{v} \quad (37)$$

159 The cavity contraction process for the present problem is actually in a self-similar manner that all soil
 160 particles share the same stress and deformation paths (Chen and Abousleiman 2013; Chen and Abousleiman
 161 2016). Hence, stresses/strains in the Eulerian description can be transformed into those in the Lagrangian
 162 description by auxiliary variables (e.g. $(r-r_0)/r$ and r_0/r) (Chen and Abousleiman 2013; Su 2021). In this
 163 letter $\ln(r/r_0)$ is involved as a new auxiliary variable, which can further simplify the derivation than former
 164 auxiliary variables. The incremental forms of $\ln(r/r_0)$ in terms of Lagrangian and Eulerian descriptions
 165 equal each other owing to the self-similar characteristic (i.e. $d[\ln(r/r_0)] = D[\ln(r/r_0)]$), thereby giving

$$166 \quad \frac{Dr}{r} = \frac{dr}{r} - \frac{dr_0}{r_0} \quad (38)$$

167 Combining Eqs. (37) and (38), we can get

$$168 \quad \frac{dr}{r} = \frac{1}{1-(r/r_0)^2} \left(\frac{v_0}{v} \right) \frac{Dr}{r} \quad (39)$$

169 Then the equilibrium equation (1) can be rewritten in the Lagrangian description by substituting Eqs. (4), (10),
 170 and (39) into Eq. (1), as

$$171 \quad D\sigma'_r + \lambda_{sc} s_0 Dv = (\sigma'_\theta - \sigma'_r) \left(\frac{r_0^2 v}{r_0^2 v - r^2 v_0} \right) \frac{Dr}{r} \quad (40)$$

172 Later, the ODEs for the elastoplastic cavity contraction process can be derived by combining Eqs. (23), (35),
 173 (36), and (40), as

$$174 \begin{bmatrix} 1 & 0 & 0 & \lambda_{se}s_0 \\ B_{r\theta} & B_{\theta\theta} & B_{z\theta} & 0 \\ B_{rz} & B_{\theta z} & B_{zz} & 0 \\ B_{rp} & B_{\theta p} & B_{zp} & 1/v \end{bmatrix} \begin{bmatrix} D\sigma'_r \\ D\sigma'_\theta \\ D\sigma'_z \\ Dv \end{bmatrix} = \frac{Dr}{r} \begin{bmatrix} \frac{\sigma'_\theta - \sigma'_r}{1 - (r/r_0)^2 (v_0/v)} \\ -1 \\ 0 \\ 0 \end{bmatrix} \quad (41)$$

175 The ODEs can be readily solved with the initial values provided by the elastic solution at the elastoplastic
 176 boundary.

177 Finally, the radius in Eq. (41) should be seen in the form of Lagrangian description. In order to
 178 investigate field distributions, it is necessary to integrate Eq. (40) to obtain the equivalent radius in the Eulerian
 179 description (Chen and Abousleiman 2013; Chen H et al. 2022):

$$180 \ln \frac{r}{a} = \int_a^r \frac{1}{1 - (r/r_0)^2 (v_0/v)} \frac{Dr}{r} \quad (42)$$

181 Results and discussion

182 Based on the similarity between cavity contraction and tunnel convergence (Brown et al. 1983; Mair and
 183 Taylor 1993; Yu 2000), the influence of soil suction on GRCs, stress paths, and stress distributions is
 184 investigated using the developed cavity contraction solution with input parameters in Table 1 (Chen H et al.
 185 2020; Chen S et al. 2020).

186 At first, finite element analyses (FEM) for cavity contraction in the dry soil (i.e. $s_0=0$) are conducted by
 187 ABAQUS 2020 following the numerical model of Yang et al. (2022), which can verify the accuracy of the
 188 proposed solution (e.g. Figure 3 and Figure 5).

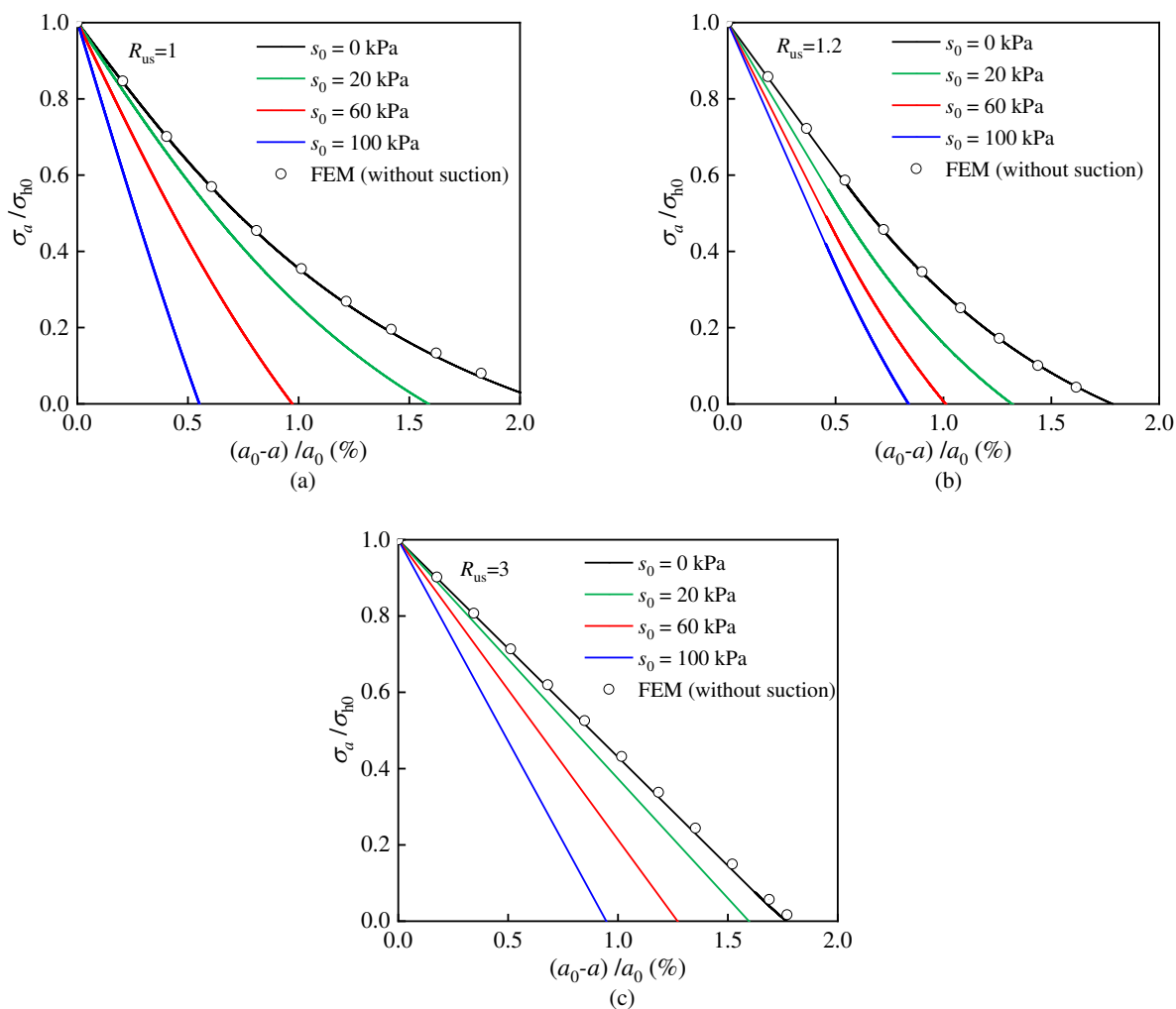
189 **Table 1 Input parameters for parametric study**

σ'_{h0} : kPa	σ'_{v0} : kPa	p'_0	K_0	S_{r0}	p'_{y0} : kPa	v_0	R_{us}
100	160	120	0.625	0.6	140.8	2.09	1
100	160	120	0.625	0.6	168.96	2.06	1.2
130	100	120	1.3	0.6	375.6	1.97	3

190 $M = 1.2$, $b = 0.65$, $c = 0.125$, $\lambda(0) = 0.15$, $\lambda_{se} = 0.21$, $\kappa = 0.03$, $\mu = 0.3$, $p'_n = 10\text{kPa}$

191 Figure 3 shows the influence of suction on the normalised GRCs with different overconsolidation ratios.

192 For a given R_{us} , it can be found that suction increase imposes an important impact on GRCs, which makes
 193 the normalised internal pressure decrease faster with tunnel convergence (i.e. $1 - a/a_0$). Moreover, GRC is
 194 much steeper for a larger R_{us} because of the hardening effect of preconsolidation, and this is consistent with
 195 the observation in Chen and Abousleiman (2016) for dry soils.



196
 197
 198 **Figure 3** Influence of suction on GRCs: (a) $R_{us} = 1$; (b) $R_{us} = 1.2$; (c) $R_{us} = 3$

199 To further explore the suction effect, Figure 4 plots the stress paths for a soil particle at $r = a$ in the
 200 normalised $p' - q$ plane. These paths end at the occasion when the internal support pressure decreases to
 201 zero (i.e. $\sigma_a = 0$, marked by solid squares). Comparing the stress paths during cavity contraction in
 202 unsaturated and dry soils (Figure 4), two main features can be observed:

- 203 (a) The particle for unsaturated soils goes a much shorter stress path than that in dry soils. In fact, the
 204 effective radial stress at $r = a$ can be expressed as $\sigma'_r = \sigma_a + S_r s_0 > 0$ for unsaturated soils (see Eq.

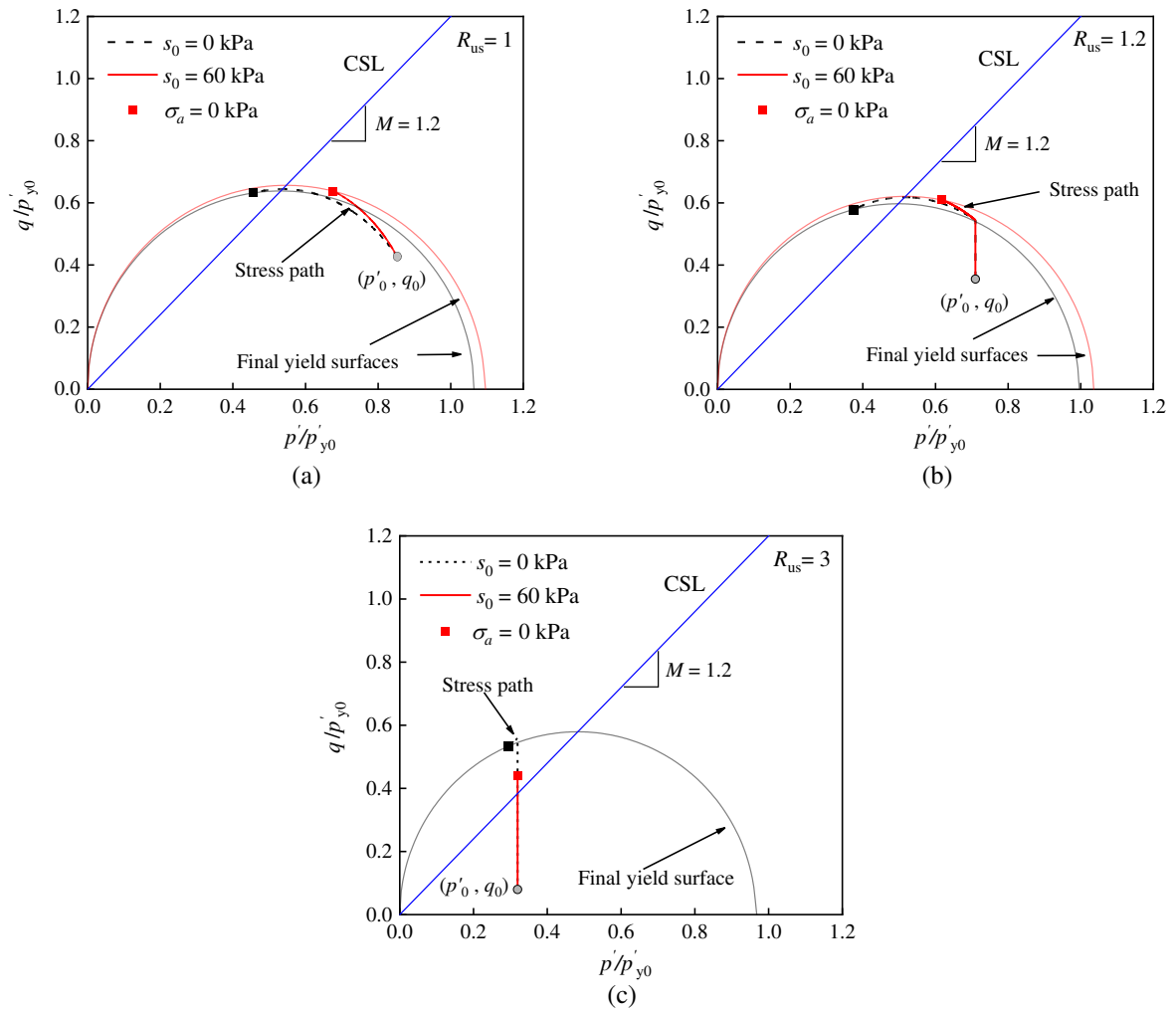
205
206
207
208
209
210

(4)), while $\sigma'_r = \sigma_a = 0$ for soils without suction. Therefore, the suction effect on the effective stress is an important reason for the shorter stress paths in the $p'-q$ plane.

(b) After yielding occurs, unsaturated soils can bear a higher deviatoric stress at the same p' and R_{us} .

This is because soil suction leads to the expansion of yield surfaces (see Eq. (7) and Figure 2).

Accordingly, the suction effect on effective stresses and yield surfaces is also the reason for the variation of GRCs with soil suction.

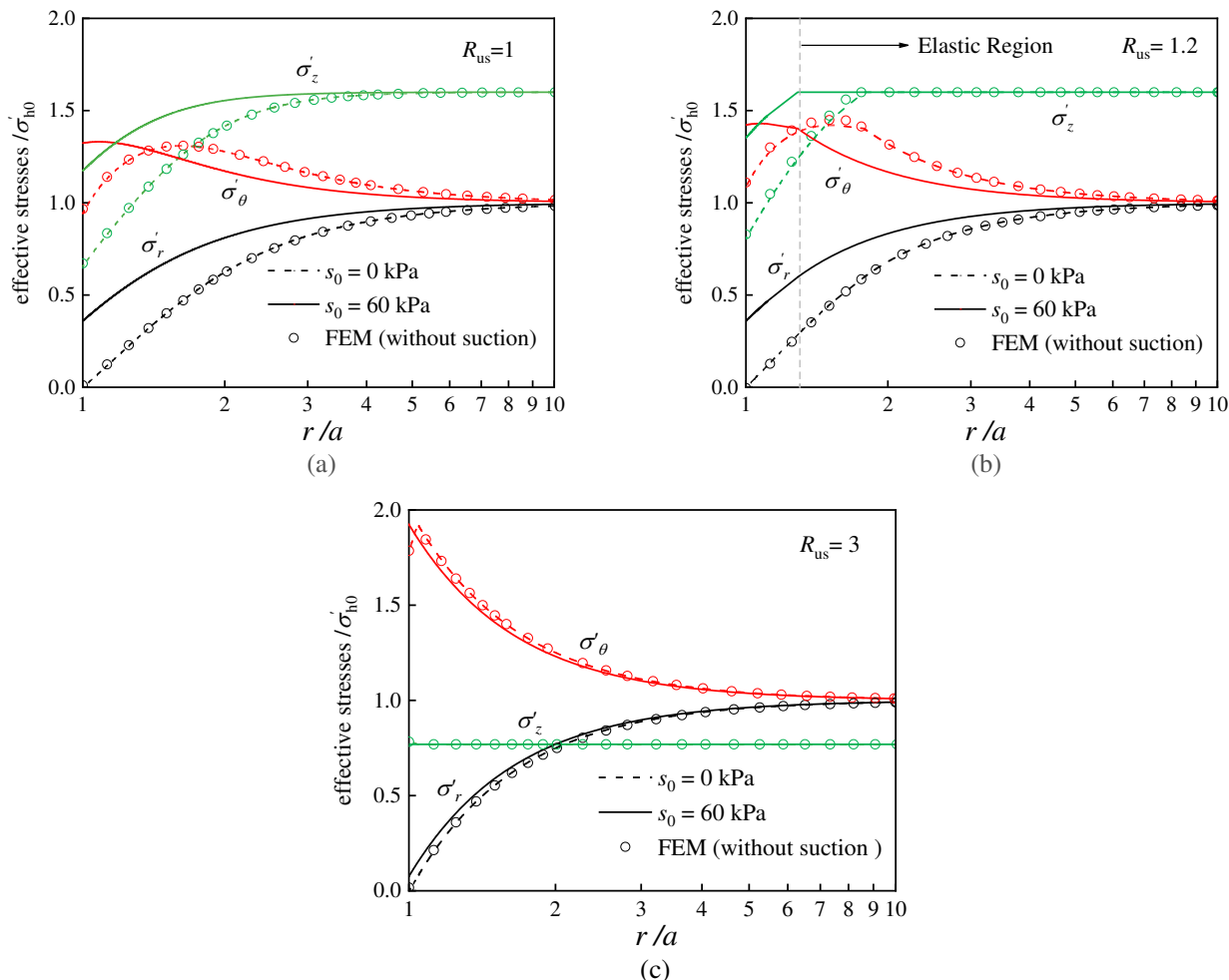


211
212
213
214
215
216
217

Figure 4 Stress paths for unsaturated and dry soils: (a) $R_{us}=1$; (b) $R_{us}=1.2$; (c) $R_{us}=3$

Figure 5 shows the distributions of effective radial, circumferential, and vertical stresses at the occasion of $\sigma_a = 0$. For unsaturated soils the effective radial stress at $r = a$ is positive instead of reducing to zero, which is consistent with $\sigma'_r = \sigma_a + S_r s_0 > 0$. When compared with the case without suction, the unloading-induced plastic zone becomes narrower for unsaturated ground, but the maximum circumferential effective

218 stress tends to be larger. Hence, the stress distribution results indicate that the effective stresses are not fully
 219 released due to the suction effect in unsaturated soils. In the long-time period when soils are wetted (i.e. suction
 220 decrease), stress redistribution may occur around tunnels and the unloading-induced plastic zone may expand
 221 further.



222

223

224

Figure 5 Stress distributions for unsaturated and dry soils: (a) $R_{us} = 1$; (b) $R_{us} = 1.2$; (c) $R_{us} = 3$

225

Conclusions

226

227

228

229

230

231

232

An elastoplastic solution is developed for cavity contraction in unsaturated soils under constant suction conditions to investigate the influence of soil suction on GRCs. The equilibrium equation, constitutive equations for unsaturated soils, and continuity equation for the cavity contraction problem are transformed into a system of first-order ODEs by introducing a new auxiliary variable. After validating the solution accuracy, the effects of soil suction and overconsolidation ratio on GRCs, stress paths, and stress distributions are investigated. It is found that for a larger suction and overconsolidation ratio, the internal support pressure reduces faster with tunnel convergence. The soil particle for unsaturated soils goes a shorter stress path due to

233 the influence of suction on effective stresses and yield surfaces. Finally, stress distributions indicate that the
 234 effective stresses around unsaturated tunnels may not be fully released. The proposed solution can also be
 235 useful for wellbore drilling problems in unsaturated soils.

236 **Acknowledgement**

237 We would like to acknowledge the financial support from the National Natural Science Foundation of China
 238 (52108374), the “Taishan” Scholar Program of Shandong Province, China (tsqn201909016), the Shandong
 239 Provincial Natural Science Foundation (ZR202102250562), and the Key Basic Research Project of China
 240 (No.2022YFC3005604). The last author would also like to thank the financial support from the China
 241 Scholarship Council for his study at the University of Leeds.

242 **Notation List**

a, a_0	initial and current radius of cavity wall
b, c	material parameters for unsaturated soils
$D(\bullet), d(\bullet)$	material time and spatial differentials of (\bullet)
E	Young’s modulus
f	yield function
M	slope of critical state line
p'_0, p'	initial and current effective mean stress
$p'_y(0), p'_y(s)$	yield stresses for saturated and unsaturated soils
p'_{y0}	initial isotropic pre-consolidation stress
q, q_0, q_p	deviator stress, initial deviator stress, and deviator stress at the elastoplastic boundary
r_0, r	initial and current radial positions of a soil particle
R_{us}	overconsolidation ratio
s_0, s	initial and current suction
S_{r0}, S_r	initial and current degree of saturation
u	radial displacement of a soil particle
u_a, u_w	pore air and water pressures
v_0, v	initial and current specific volumes
$\varepsilon_r^e, \varepsilon_\theta^e, \varepsilon_z^e$	elastic radial, circumferential and vertical strains
$\varepsilon_r, \varepsilon_\theta, \varepsilon_z$	radial, circumferential and vertical strains

$\varepsilon_v, \varepsilon_v^p$	total and plastic volumetric strains
K	slope of loading–reloading line in $v - \ln p'$ plane
$\lambda(0), \lambda(s)$	slopes of the normal compression lines for saturated and unsaturated soils
λ_{se}	slope of the $S_r - v$ curve at constant suction
μ	Poisson's ratio of soil
ρ_0, ρ	initial and current radii of elastic-plastic boundary
η	stress ratio
σ_a	inner cavity pressure
σ_{h0}, σ_{v0}	in-plane and out-of-plane in-situ stress
$\sigma'_{h0}, \sigma'_{v0}$	in-plane and out-of-plane effective in-situ stress
$\sigma_r, \sigma_\theta, \sigma_z$	total radial, circumferential, and vertical stresses
$\sigma'_r, \sigma'_\theta, \sigma'_z$	effective radial, circumferential, and vertical stresses

243

References

244

Alonso, E. E., Gens, A. and Josa, A. (1990). "A constitutive model for partially saturated soils." *Géotechnique* **40**(3): 405-430.

245

246

Brown, E. T., Bray, J. W., Ladanyi, B. and Hoek, E. (1983). "Ground response curves for rock tunnels." *Journal of Geotechnical Engineering* **109**(1): 15-39.

247

248

Cai, W., Zhu, H., Liang, W., Wang, X., Su, C. and Wei, X. (2023). "A post-peak dilatancy model for soft rock and its application in deep tunnel excavation." *Journal of Rock Mechanics and Geotechnical Engineering* **15**(3): 683-701.

249

250

251

Carranza-Torres, C. (2003). "Dimensionless graphical representation of the exact elasto-plastic solution of a circular tunnel in a Mohr-Coulomb material subject to uniform far-field stresses." *Rock Mechanics and Rock Engineering* **36**(3): 237-253.

252

253

254

Chen, H., Feng, C. and Li, J. (2022). "An anisotropically elastoplastic solution to excavation responses of a circular opening considering three-dimensional strength." *Acta Geotechnica* **17**(9): 3995-4011.

255

256

Chen, H., Li, L. and Li, J. (2020). "Elastoplastic solutions for cylindrical cavity expansion in unsaturated soils." *Computers and Geotechnics* **123**: 103569.

257

258

Chen, S., Abousleiman, Y. and Muraleetharan, K. (2012). "Closed-form elastoplastic solution for the wellbore problem in strain hardening/softening rock formations." *International Journal of Geomechanics* **12**(4): 494-507.

259

260

261

Chen, S., Abousleiman, Y. and Muraleetharan, K. K. (2022). "Computational implementation of bounding surface model and its verification through cavity benchmark problems." *International Journal for Numerical and Analytical Methods in Geomechanics* **46**(3): 553-569.

262

263

264

Chen, S., Li, L. and Zhang, Z. (2020). *Analysis of Cylindrical Cavity Expansion in Partially Saturated Soils*. Geo-Congress 2020: Geo-Systems, Sustainability, Geoenvironmental Engineering, and Unsaturated Soil Mechanics, American Society of Civil Engineers Reston, VA.

265

266

267

Chen, S. L. and Abousleiman, Y. N. (2013). "Exact drained solution for cylindrical cavity expansion in

- 268 modified Cam Clay soil." Géotechnique **63**(6): 510-517.
- 269 Chen, S. L. and Abousleiman, Y. N. (2016). "Drained and undrained analyses of cylindrical cavity contractions
270 by bounding surface plasticity." Canadian Geotechnical Journal **53**(9): 1398-1411.
- 271 Chen, S. L. and Abousleiman, Y. N. (2017). "Wellbore stability analysis using strain hardening and/or
272 softening plasticity models." International Journal of Rock Mechanics and Mining Sciences **93**: 260-268.
- 273 Guan, K., Zhu, W., Yu, Q., Cui, L. and Song, F. (2022). "A plastic-damage approach to the excavation response
274 of a circular opening in weak rock." Tunnelling and Underground Space Technology **126**: 104538.
- 275 Ma, Y., Zhu, H., Cai, W., Su, C. and Wei, X. (2023). "Analytical method for elastic-brittle-plastic analysis of
276 a circular tunnel in a non-hydrostatic in-situ stress field considering the unified strength criterion."
277 Applied Mathematical Modelling **121**: 780-799.
- 278 Mair, R. J. and Taylor, R. N. (1993). Prediction of clay behaviour around tunnels using plasticity solutions.
279 Predictive Soil Mechanics: Proceedings of the Wroth Memorial Symposium, Oxford, UK, Thomas
280 Telford.
- 281 Mo, P.-Q. and Yu, H.-S. (2017). "Undrained Cavity-Contraction Analysis for Prediction of Soil Behavior
282 around Tunnels." International Journal of Geomechanics **17**(5): 04016121.
- 283 Park, K.-H., Tontavanich, B. and Lee, J.-G. (2008). "A simple procedure for ground response curve of circular
284 tunnel in elastic-strain softening rock masses." Tunnelling and Underground Space Technology **23**(2):
285 151-159.
- 286 Su, D. (2021). "Drained solution for cylindrical cavity expansion in modified Cam Clay soil under constant
287 vertical stress." Canadian Geotechnical Journal **58**(2): 176-189.
- 288 Sun, D. a., Sheng, D. and Sloan, S. W. (2007). "Elastoplastic modelling of hydraulic and stress-strain
289 behaviour of unsaturated soils." Mechanics of Materials **39**(3): 212-221.
- 290 Sun, Z., Zhang, D., Fang, Q., Wang, J., Chu, Z. and Hou, Y. (2023). "Analysis of interaction between tunnel
291 support system and surrounding rock for underwater mined tunnels considering the combined effect of
292 blasting damage and seepage pressure." Tunnelling and Underground Space Technology **141**: 105314.
- 293 Vrakas, A. and Anagnostou, G. (2014). "A finite strain closed - form solution for the elastoplastic ground
294 response curve in tunnelling." International Journal for Numerical and Analytical Methods in
295 Geomechanics **38**(11): 1131-1148.
- 296 Xu, C. and Xia, C. (2021). "A new large strain approach for predicting tunnel deformation in strain-softening
297 rock mass based on the generalized Zhang-Zhu strength criterion." International Journal of Rock
298 Mechanics and Mining Sciences **143**: 104786.
- 299 Yang, C., Chen, H. and Li, J. (2022). "Analysis of undrained cylindrical cavity contraction in anisotropic soils
300 under constant total vertical stress condition." European Journal of Environmental and Civil Engineering:
301 1-18.
- 302 Yu, H.-S. (2000). Cavity expansion methods in geomechanics, Kluwer Academic Publishers, Dordrecht, The
303 Netherlands.
- 304 Yu, H.-S. and Houlsby, G. T. (1991). "Finite cavity expansion in dilatant soils: loading analysis." Géotechnique
305 **41**(2): 173-183.
- 306 Yu, H.-S. and Rowe, R. K. (1999). "Plasticity solutions for soil behaviour around contracting cavities and
307 tunnels." International Journal for Numerical and Analytical Methods in Geomechanics **23**(12): 1245-
308 1279.
- 309 Zareifard, M. R. (2020). "A new semi-numerical method for elastoplastic analysis of a circular tunnel
310 excavated in a Hoek-Brown strain-softening rock mass considering the blast-induced damaged zone."
311 Computers and Geotechnics **122**: 103476.

- 312 Zhao, Y., Wei, T., Wang, C. and Bi, J. (2023). "A New Close-Form Solution for Elastoplastic Seepage-Induced
313 Stresses to Circular Tunnel with Considering Intermediate Principal Stress." Rock Mechanics and Rock
314 Engineering **56**(9): 6545-6557.
- 315 Zhuang, P.-Z., Yang, H., Yue, H.-Y., Fuentes, R. and Yu, H.-S. (2022). "Plasticity solutions for ground
316 deformation prediction of shallow tunnels in undrained clay." Tunnelling and Underground Space
317 Technology **120**: 104277.
- 318 Zhuang, P.-Z., Yu, H.-S., Mooney, S. J. and Mo, P.-Q. (2020). "Loading and unloading of a thick-walled
319 cylinder of critical-state soils: large strain analysis with applications." Acta Geotechnica **16**(1): 237-261.
- 320